

Article

# Fabrication of Self-healing Superhydrophobic Surfaces from Water-Soluble Polymer Suspensions Free of Inorganic Particles through Polymer Thermal Reconstruction

Yalun Shen, Yitian Wu, Zhehong Shen \* and Hao Chen \*

Department of Engineering, Zhejiang Agriculture and Forestry University, Hangzhou 311300, China; s841734857@163.com (Y.S.); timwuyt@163.com (Y.W.)

\* Correspondence: 19990010@zafu.edu.cn (Z.S.); haochen10@fudan.edu.cn (H.C.)

Received: 11 March 2018; Accepted: 11 April 2018; Published: 16 April 2018



**Abstract:** Self-healing superhydrophobic surfaces have been fabricated by casting and drying water-soluble amphiphilic polymer suspensions at room temperature through thermal reconstruction. When compared with previous methods, this approach exploits modified natural hierarchical microstructures from wood instead of artificially constructing them for superhydrophobic morphology, which involves neither organic solvent nor inorganic particles nor complex procedures. The obtained superhydrophobic surface has acceptable resistance to abrasion. The surface can recover superhydrophobicity spontaneously at room temperature upon damage, which can be accelerated at a higher temperature. After depleting healing agents, the polymer suspension can be sprayed or cast onto wood surfaces to replenish healing agents and to restore self-healing ability. The superhydrophobic surface greatly increases the mold inhibition and water resistance of wood, which would prolong the service life of wood based materials.

**Keywords:** superhydrophobic surfaces; water-soluble polymers; natural hierarchical microstructures; polymer thermal reconstructions

## 1. Introduction

The fabrication of superhydrophobic surfaces has attracted extensive interests over the past few years due to its great potential both in theoretical research and practical applications, such as durable antibacterial action [1–4], screen filter [5], antifouling [6], gas sensing and droplet manipulation [7], oil/water separation [8,9], self-cleaning [10], and antireflection [11]. The superhydrophobic property of the surface is governed by its chemical compositions and geometric microstructures. The combinations of hierarchical microstructures with low-surface energy materials have been the main strategy for fabricating superhydrophobic surfaces. In general, superhydrophobic surfaces can be obtained by enhancing the roughness of hydrophobic surfaces. Therefore, many methods have been developed to improve the roughness of solid surfaces to fabricate superhydrophobic surfaces, such as plasma polymerization/etching [12,13], chemical vapor deposition [14,15], solvent-mediated phase separation [16], solvent-free or wet chemical free approaches [17,18], and polymer self-assembly [19–21]. Although many physical and chemical methods have been developed to fabricate superhydrophobic surfaces, the lack of cheap fabrications, mechanical robustness, and self-replenishment upon damage once have remained as the main obstacles for the widespread applications of some superhydrophobic surfaces since an artificially fragile surface texture can be damaged by scratches, abrasions, or even brief contacts with fingers, which made them apt to lose superhydrophobicity. However, up to

date, through extensive efforts, many achievements have been made to fabricate mechanical durable superhydrophobic surfaces [22–26], which helps in applying them in practical applications.

Polymers without solvent and inorganic matter through tribocharging [17,18] or with solvent and inorganic matter through high temperature melting for thermal reconstructions [27] have been used to fabricate robust superhydrophobic surfaces, which are highly efficient, rapid, and inexpensive. In the present study, the superhydrophobic surfaces from unitary water-soluble polymer suspensions were obtained through polymer thermal reconstruction by taking advantage of natural hierarchical microstructures just by sanding wood, instead of artificially constructing them for superhydrophobic morphology. The whole process did not involve toxic organic solvents, inorganic particles, or complex procedures. The water CA with  $152^\circ$  was obtained at room temperature, which was smaller than the water CAs  $164^\circ$  for some polymer superhydrophobic surfaces [17]. When compared with the excellent abrasion resistance of some polymer superhydrophobic surfaces, which could maintain its superhydrophobicity under the pressure of 17.5 KPa with 15 abrasion cycles [27] or mechanical stability after 100 abrasion cycles with sandpaper [17], the obtained superhydrophobic surfaces in the present had acceptable level of mechanical properties, which could maintain its superhydrophobicity under the pressure of 3.5 KPa with nine abrasion cycles. However, even the most durable superhydrophobic surface would eventually become damaged by the repeated mechanical abrasion or chemical etching, which would damage its low surface energy material or texture. Hence, a superhydrophobic surface that could recover superhydrophobicity upon damage would be highly desirable [7,28–40]. Based on the intrinsic porous morphology of wood surfaces, superhydrophobic coatings can preserve a large number of amphiphilic polymers as healing agents in wood pores, such as cell cavities and grooves. Once the primary top polymer layer is decomposed or scratched, the preserved healing agents in cell cavities and grooves can migrate to wood surfaces driven by minimum interfacial energy at ambient temperature [31]. Furthermore, healing agents, which cooperate with robust porous structures that are not easily destroyed and are essential for the recovering of the superhydrophobicity, result in the self-healing of the superhydrophobicity. Furthermore, after depleting healing agents, the polymer suspensions could be sprayed or cast onto wood surfaces to replenish healing agents and restore its self-healing ability. These reported principles can be extended towards the self-healing of other surface-dependent functionalities, such as anti-mildew or anti-water, which will remain high performance levels all through their life-cycle with low cost and energy demand for maintenance and surface repairs.

As renewable resources, wood has great potential in furniture and decoration materials that can take the place of steel, stone, and glass, due to the forthcoming exhaustion of un-renewable resources, such as petroleum, coal, and minerals [41–43]. However, as a natural hygroscopic polymer composite with many hydrophilic groups such as hydroxyl groups (–OH), wood is apt to absorb water, which would result in dimension instability and microorganism attacks from decay fungi or mold. This would greatly reduce its service life. Improvement in the water repelling of wood is an effective way to prevent the harmful effects from water. Many methods have been put forward to improve the hydrophobicity of wood [44–47], which would help to apply them in practice. The method free of inorganic particles in the present study greatly improves the hydrophobicity of wood without varying its surface textures. Therefore, this approach to robust superhydrophobic surfaces is not only important for technologies, which avoids organic solvents, surfactants, and the application of complex methods, but it also opens up a new way to modify wood with better water and mildew resistance without inorganic particles.

## 2. Experimental Section

### 2.1. Materials

Butyl acrylate (BA), styrene (St), acrylic acid (AA), and ammonium persulfate (APS), were purchased from Shanghai Chemical Reagent Co. (Shanghai, China). Allyloxy hydroxypropyl

sodium sulphonate (HAPS, 40 wt % of solid content in aqueous solution) was kindly donated by Guangzhou Shuangjian Trading Co., Ltd. (Guangzhou, China). Chinese-fir wood and hexafluorobutyl acrylate (FBA) were kindly donated by Zhejiang Longyou Wood Bond Co. (Quzhou, China). Wood blocks of 40 mm × 35 mm × 10 mm (longitudinal × radial × tangential) were obtained from the sapwood of Chinese fir (*Cunninghamia lanceolata*). The wood was sanded with 240 grit sandpaper before its coating, unless other specified. Deionized water was used in all of the polymerizations. All of the chemical reagents were used without further purification.

## 2.2. Synthesis of Colloidal Polymer Spheres

A typical surfactant-free emulsion polymerization procedure was carried out, as follows: deionized water (80 g), HAPS (1 g), AA (1g), FBA (1g) BA (5 g), St (5 g), and APS (0.05 g) were added sequentially into a four-necked flask equipped with an N<sub>2</sub> inlet, a reflux condenser, and a mechanical stirrer at a stirring speed of 150 rpm. The polymerization was initially performed at 75–80 °C for 2 h and added with a mixture of AA (1 g), BA (15 g), St (15 g), and APS (0.2 g dissolved in 15 g of water) over a period of 2 h, sequentially. The reaction was allowed to proceed for another 6 h to obtain water-soluble polymer latex with a solid content of 34 wt %. The glass transition temperature of polymer is 30 °C measured by differential scanning calorimeter (DSC), unless other specified.

## 2.3. Fabrication of Superhydrophobic Surfaces

The above polymer latexes were firstly stirred and then drop-cast onto sanded wood surfaces. The superhydrophobic surface was obtained when the latexes was dried at 30 °C.

## 2.4. Characterization

The radial surface morphology of the wood was characterized by scanning electronic microscopy (SEM, SU-8010, Hitachi High-Technologies Corporation, Tokyo, Japan). All of the samples were coated with gold by sputtering prior to observation. The size and size distribution of polymer spheres was measured by TEM images with Hitachi H-600 TEM (Hitachi, Tokyo, Japan). Digital pictures were captured using Cannon Power Shot A 95 (Cannon, Tokyo, Japan). The size distribution and zeta potential of the polymer spheres were measured by the Zeta PALS BI-90 plus (Brookhaven Instruments Corporation, Holtsville, NY, USA). The test was repeated three times. The  $T_g$  of the as-prepared sample was analyzed using a Perkin–Elmer DSC 7 (Perkin-Elmer, Waltham, MA, USA). Three-dimensional VK-X optical laser microscope system (3D OPM, Oxford Performance Materials Inc., South Windsor, CT, USA) was used to observe the optical images of the wood surface. The roughness factor ( $R_a$ ) was calculated according to JIS B0601:1994 [48]. The wettability of the surface was performed by a dynamic contact angle (CA) testing instrument (OCA40, DataPhysics, Filderstadt, Germany). CA was recorded at 30 s after a droplet of liquids (5  $\mu$ L) was placed on the surface. The sliding angle (SA) was measured by recording the tilt angle of the sample platform, at which a droplet of liquids (10  $\mu$ L) starts to roll off the surface. The average water CA was obtained on cross sections by measuring the same wood sample at six different positions. Fourier Transform infrared spectroscopy (FTIR) measurements were carried out with a Nicolet Nexus 470 spectrometer (Thermo Fisher Scientific, Waltham, MA, USA) with a resolution of 0.5  $\text{cm}^{-1}$  for 32 scans. The dried powder of the wood surface was blended with KBr to prepared pellets for examinations. The surface composition of the wood surface was measured by X-ray photoelectron spectroscopy (XPS, Perkin-Elmer PHI 5000C ECSA, Perkin-Elmer, Waltham, MA, USA) using Al K radiation at a 90 take-off angle. All of the binding energy value was calibrated using the reference peak of C 1s at 284.7 eV. The abrasion resistance of the superhydrophobic wood surface was evaluated by dragging a piece of 240 grit sandpaper under 500 g weights in one direction with a speed of 1  $\text{cm}\cdot\text{s}^{-1}$  at a distance of 10 cm per cycle. Unless specified, the characterizations, such as SEM, OPM, Water CA, FTIR, XPS, and abrasion tests were carried out on the radial section of wood blocks.

### 3. Results and Discussion

#### 3.1. Synthesis and Morphology of Water-Soluble Amphiphilic Polymer Spheres

Polystyrene-block-poly(butyl-acrylate)-block-poly(hexafluorobutyl-acrylate)-block-poly(acrylic acid) (PST-BA-HFB-AA) were synthesized by soap-free batch emulsion polymerization. The amphiphilic polymer spheres are of uniform shapes with a dark hydrophobic core representing the PS-FBA rich regions, which are surrounded by the lighter shells of the PAA-PBA-rich domains, as shown in Figure 1a. The diameter of the polymer spheres is approximately 381 nm, with 0.005 polydispersity, as shown in Figure 1b. The Zeta potential of the polymer sphere is  $-52.6$  mV, which ensures the stability of the polymer suspensions.

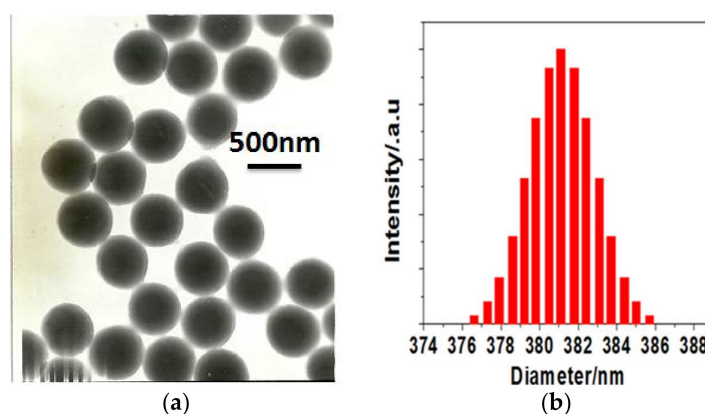


Figure 1. (a) TEM images and (b) size distributions of polymer spheres.

#### 3.2. The fabrication of Superhydrophobic Surfaces through Polymer Thermal Reconstruction and the Effect of Surface Roughness on Wettability

The raw wood without sanding (USR) has natural and uneven hierarchical structures (Figure 2a), with a maximum height of more than  $400\ \mu\text{m}$  (Figure 2b). The roughness factor ( $R_a$ ) was  $56\ \mu\text{m}$  calculated according to JIS B0601:1994 [48], which was not applicable for superhydrophobic morphology. The natural and uniform hierarchical structures that were applicable for superhydrophobic morphology are obtained simply by sanding wood with 240 grit sandpapers (SR-240) (Figure 2c), with a maximum height of less than  $100\ \mu\text{m}$  (Figure 2d) and a roughness factor ( $R_a$ ) of  $6.46\ \mu\text{m}$ . Then, the homogeneous water latex is cast onto SR-240 wood surfaces and is dried at ambient temperatures for a certain amount of time to form superhydrophobic surfaces, as shown in Scheme 1.

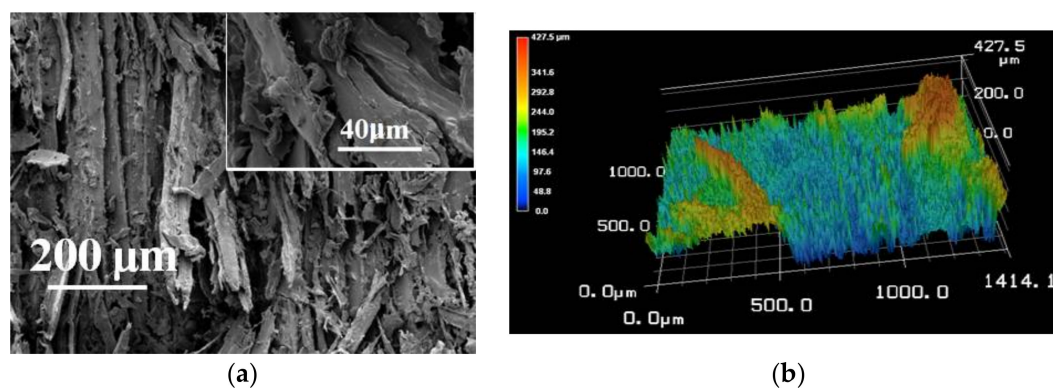
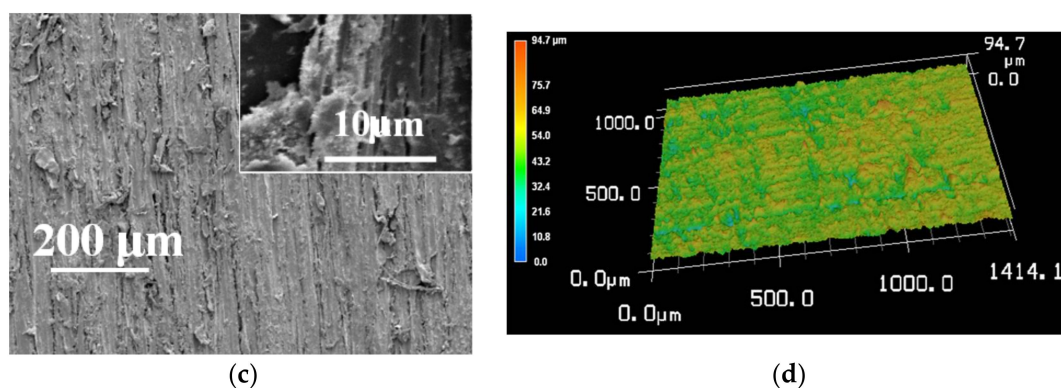
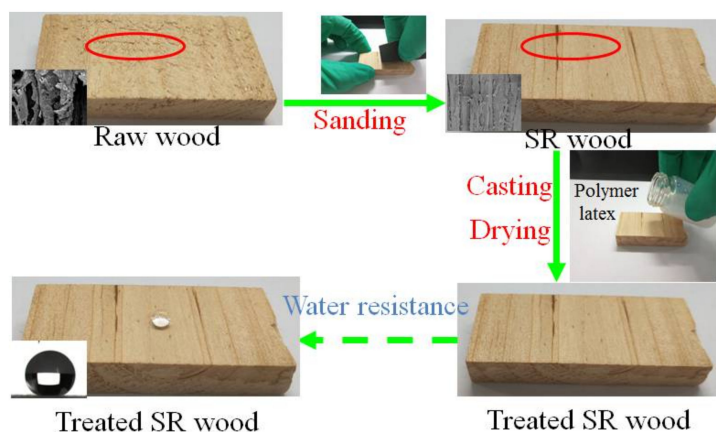


Figure 2. Cont.



**Figure 2.** (a) Scanning electronic microscopy (SEM) and (b) optical laser microscope system (OPM) images of raw wood without sanding (USR) wood. (c) SEM and (d) OPM images of SR-240 wood. The insets in (a) and (c) are the magnified SEM images.



**Scheme 1.** Schematic procedure for the preparation of superhydrophobic surfaces.

Since the raw wood have hierarchical microstructures [49] and many hydrophilic groups, such as  $-OH$  and  $C=O$  groups (Figure 3a), the surface of SR-240 wood is hydrophilic. The surface turns from hydrophilicity into superhydrophobicity with  $152^\circ$  water CAs after the water-soluble polymer suspensions are drop cast onto SR-240 wood surfaces and are dried at room temperature (Figure 3b). The wettability is relative to the effects of both surface chemical compositions and surface roughness. In order to demonstrate the change in the chemical component on SR-240 wood surfaces from hydrophilic to hydrophobic, which is responsible for its wettability transition, the FTIR spectra are examined on SR-240 wood surfaces (Figure 3c). The absorbance band at  $1733\text{ cm}^{-1}$  was ascribed to the hydrophilic groups ( $C=O$  groups from wood lignin and polymers), and the absorbance band at  $696\text{ cm}^{-1}$  was ascribed to the hydrophobic groups (benzene groups from the polymers) [21]. For SR-240 wood, there was absorbance at  $1733\text{ cm}^{-1}$ , but no absorbance at  $696\text{ cm}^{-1}$ . For the coated SR-240 wood with  $152^\circ$  water CAs, there was absorbance at  $696$  and  $1733\text{ cm}^{-1}$ . The absorption at  $696\text{ cm}^{-1}$  had proven the existence of benzene groups from the polymers on SR-240 wood surfaces. The absorption of  $CF_3$  or  $CF_2$  was not observed, probably because the group number was not enough for the examination. It was just the addition of the hydrophobic benzene group from the polymers onto SR-240 wood surface that made it hydrophobic. Therefore, the changes in the chemical components on SR-240 wood surfaces resulted in its wettability transition. A possible illustration of these chemical component changes on the coated SR-240 wood surface is that the change mainly results from the phase separation of polymer segments driven toward the minimum interfacial energy: the hydrophilic groups ( $1733\text{ cm}^{-1}$ ,  $C=O$  groups) tend to shield from the apolar air and shrink toward the interior of the polymer spheres,

while the hydrophobic groups ( $696\text{ cm}^{-1}$ , benzene groups) tend to extend toward the apolar air. Hence, the resultant surface was water repellent [20].

On the other hand, the natural and uniform roughness on wood surfaces was the other important factor that governed wettability. In order to illustrate the effect of surfaces roughness on wettability, the same polymer latex was drop cast and dried on USR wood and the raw wood sanded with 60 grit sandpapers (SR-60) and 320 grit sandpapers (SR-320) under the same conditions, respectively. The results in Figure 3d show that the water CAs on USR wood, SR-60 wood, and SR-320 wood were  $136^\circ$ ,  $140^\circ$ , and  $147^\circ$ , respectively, which were smaller than those ( $152^\circ$ ) on SR-240 wood. For SR-60 wood, although hierarchical microstructures were present, these microstructures were uneven with the roughness factors ( $R_a$ )  $13\text{ }\mu\text{m}$  (Figure 4a,b). The pore size on USR and SR-60 wood surface greatly varied. Some pores (grooves) were so large that the comprehensive force on the contact lines could not support the weight of the water droplet, and the water droplet penetrated and filled the pores. Therefore, the wetting behavior was homogeneous, which was in the Wenzel regime. In the Wenzel regime, the coated surface was not a superhydrophobic surface with CA hysteresis that was larger than  $10^\circ$ . For SR-240 wood, the roughness factors were  $6.46\text{ }\mu\text{m}$  and the pores were small and uniform. The comprehensive force on the contact lines could support the weight of the water droplet, allowing for the water droplet to sit on the crests of the rough surfaces. Hence, the wetting behavior was in the Cassie-Baxter regime. Therefore, the coated surface on SR-240 wood approached the superhydrophobic state with CA hysteresis as  $4^\circ$ . When the sandpaper mesh further increased to 320 grit, the wood surface was smoother with the roughness factors as  $5.6\text{ }\mu\text{m}$  (Figure 4c). The pores were smaller and fewer (Figure 4d) that the air in contact lines reduced. Hence, the water CAs decreased to  $147^\circ$  with CA hysteresis as  $15^\circ$ . Therefore, the surface roughness on SR-240 wood was the most appropriate for superhydrophobic morphology.

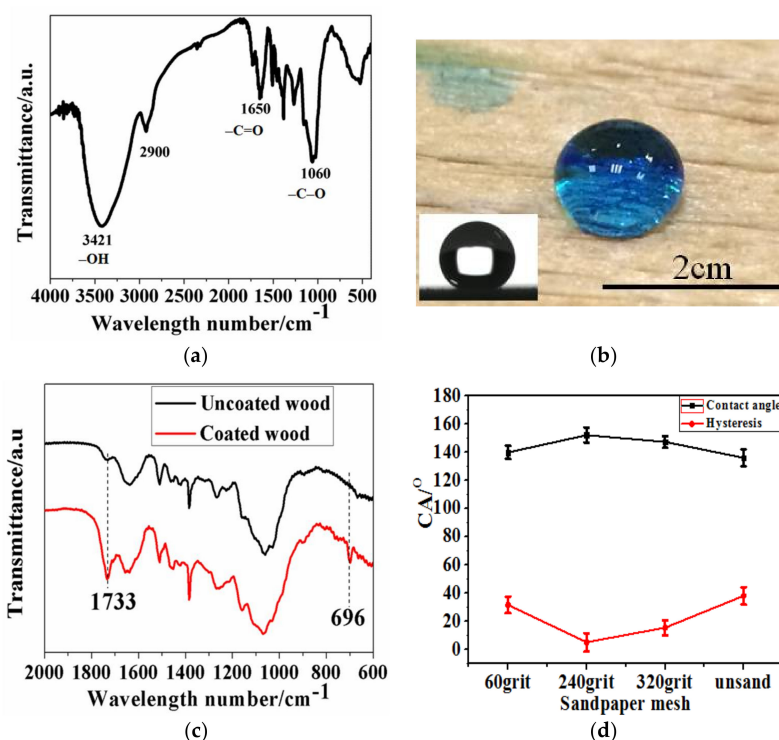


**Figure 3.** (a) FTIR spectra of the uncoated SR-240 wood; (b) Water contact angles (CAs) of the coated SR-240 wood; (c) FTIR spectra of the uncoated SR-240 wood and the coated SR-240 wood; (d) The effect of sandpaper mesh on water CAs.

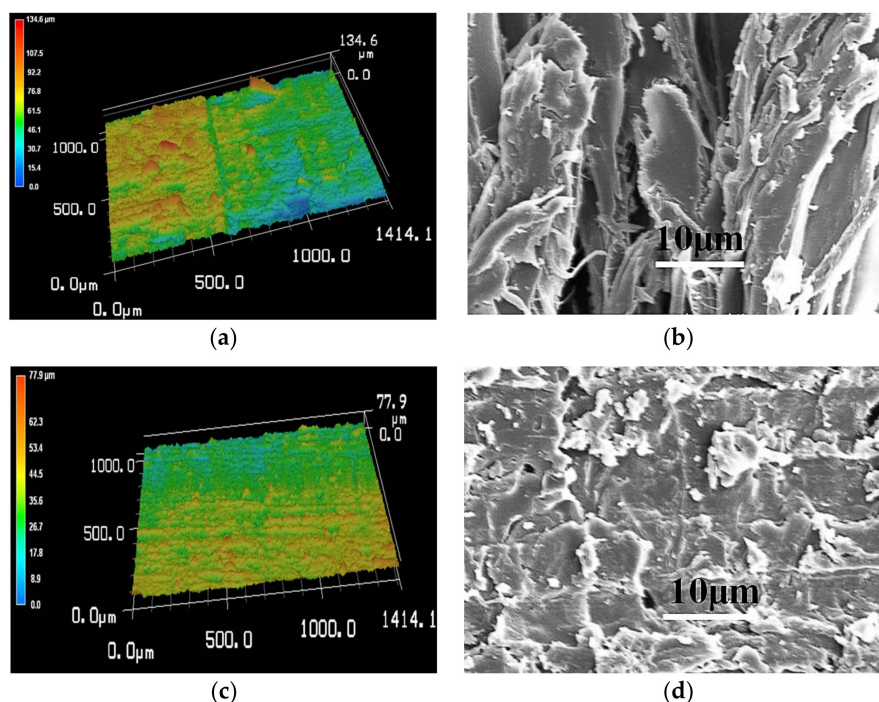


**Figure 4.** (a) OPM and (b) SEM images of SR-60 wood. (c) OPM and (d) SEM images of SR-320 wood.

### 3.3. Effect of ST/BA Mass Ratio on Wettability

With the constant fabrication temperature being set at 30 °C, the ST/BA mass ratio has great effects on wettability, as shown in Figure 5a. The corresponding water CAs were 152°, 122°, 109°, and 60° when the ST/BA mass ratio was 1.0, 1.5, 5.8, and 10.0, respectively. As shown in the above illustration, the critical feature of the transition of wood surfaces from hydrophilic to superhydrophobic was the change of the surface chemical component, which arose from the reorientation/phase separation of hydrophilic or hydrophobic polymer segments that were driven towards minimum interfacial energy. This process, called “thermal reconstruction”, tends to become harder when the segmental mobility decreases. With the ST/BA mass ratio increasing, the polymer chain is composed of more rigid PS, which restricts chain movement and contributes to high  $T_g$ . As demonstrated in Figure 5b, the polymer  $T_g$  increases from 30, 40, 70, to 85 °C when the ST/BA mass ratio increases from 1.0, 1.5, and 5.8 to 10.0 in latex spheres.

The polymer  $T_g$  determines the mobility of the polymer segments with the other conditions unvaried. When the polymer  $T_g$  (85 °C) was much higher than the fabrication temperature (30 °C), the polymer chain or segment could not move, except for the vibrations of the atoms or groups that were near the balanced positions [21,27]. The hydrophilic shells and the hydrophobic cores of the polymer spheres could not perform any movement. Eventually the hydrophilic groups that were exposed at the outside of the polymer spheres with the hydrophobic groups hidden inside the polymer spheres after the water evaporated, which resulted in surface hydrophilicity on the coated SR-240 wood with 60° water CAs. When the polymer  $T_g$  decreased to 70 °C, the polymer segments, except for the polymer chains, began to move under the hydroplastic effect of water [21]. Some hydrophobic groups, such as  $\text{CH}_2$ , moved towards the apolar air, extended, and exposed at the outside of the polymer spheres. In contrast, some hydrophilic groups were hidden inside the polymer spheres. Therefore, the surface was hydrophobic with 109° water CAs. When the polymer  $T_g$  further decreased to 40 °C, the polymer chain could move gradually in addition to the movement of polymer segments. Therefore, more hydrophobic groups moved and exposed at the outside of polymer spheres, and the surface became high hydrophobicity, with 122° water CAs. When the polymer  $T_g$  was 30 °C, the polymer chains could move or flow more freely, when combined with the plastic effect of

water, which reached the viscous state. During coagulating, melting, and film-forming, more segments obtained enough energy for movement, namely, more hydrophobic groups, such as  $\text{CH}_2$  and  $\text{CF}_2$ , moved towards the apolar air, extended, and exposed at the outside of the polymer films. Furthermore, besides phase separation or inversion, which resulted from the segmental mobility of the polymer spheres, the polymer chains could move and cover the whole wood surface to form a continuous thin film [50]. The sufficient hydrophobicity combined with the roughness from SR-240 wood surface made it superhydrophobic with  $152^\circ$  water CAs.

The XPS analysis in Figure 5c–e demonstrates the change of the chemical component distribution on SR-240 wood surfaces with different water CAs corresponding to different polymer  $T_g$ . There was a broad carbon peak with several kinds of binding energy of 284.7, 286.5, and 288.9 eV, which responded for the function groups of  $\text{CH}_2$ , C–O, and C(O)O, respectively [20]. According to the results in Figure 5c for the uncoated SR-240 wood, there is a strong peak for C–O, which holds for 60% of all C atoms. In addition, C(O)O and C–H peaks also existed, which held 6% and 34% of all C atoms, respectively. The main groups that existed on the wood surfaces were hydrophilic groups, in which hydrophilic C atoms held for 66% of all C atoms. For the coated S-240 wood with  $60^\circ$  CAs ( $85^\circ\text{C } T_g$ ), as shown in Figure 5d, there is a strong peak for C–H, which holds 60% of all C atoms. Furthermore, C–O and C(O)O peaks were also present, which held 32% and 8% of all C atoms, respectively. The hydrophobic C atoms held 60% of all C atoms. There was a strong peak for C–H groups on the coated SR-240 wood with  $152^\circ$  CAs ( $30^\circ\text{C } T_g$ ), which held 78% of all C atoms, as shown in Figure 5e. The peaks for the C–O and C(O)O groups held 12% and 10%, respectively. The hydrophobic groups of  $\text{CF}_3$ ,  $\text{CF}_2$ , and  $\text{CF}$  were not observed, which was probably because the above groups were not enough to be examined, when compared with other C groups. However, the XPS survey in Figure 5f demonstrates that the main elements on the coated SR-240 wood with  $152^\circ$  CAs were C (78%), oxygen (19%) and F (2%) as compared with those on the uncoated SR-240 wood, which were C (76%), oxygen (22%), and N (1%). This proved the existence of the F element on the superhydrophobic wood.

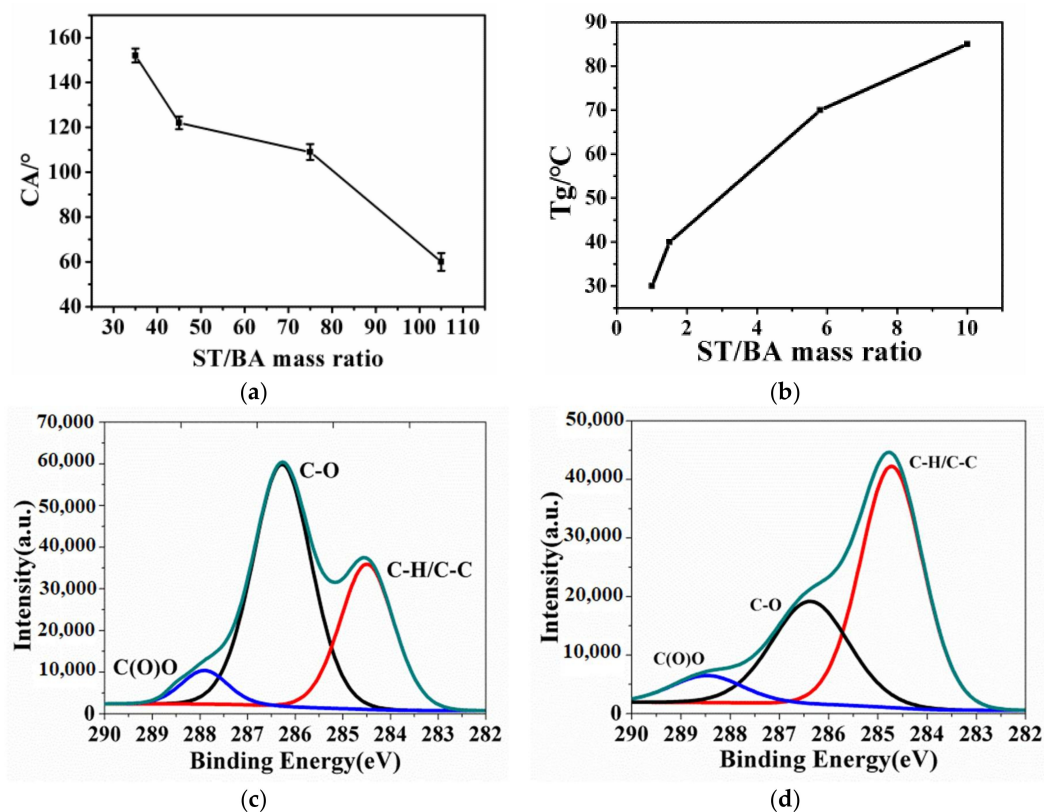
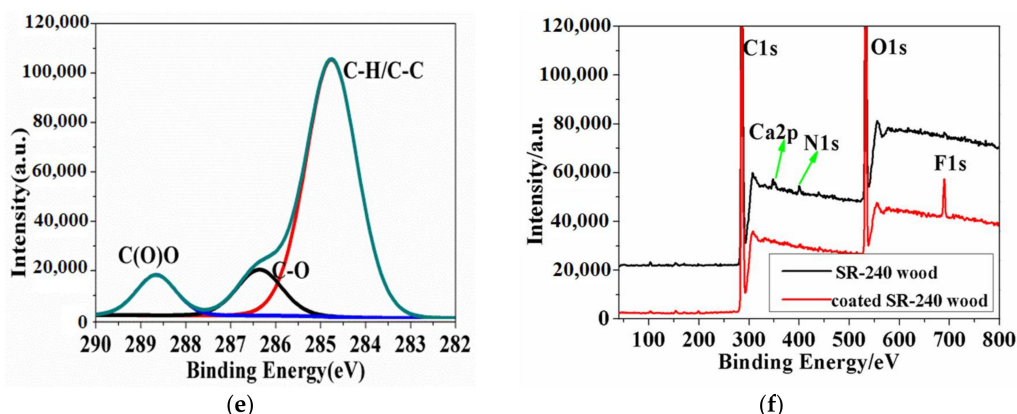


Figure 5. Cont.



**Figure 5.** (a) The effect of the styrene (ST)/butyl acrylate (BA) mass ratio on water CAs; (b) The effect of the ST/BA mass ratio on the  $T_g$  of as-prepared polymers. X-ray photoelectron spectroscopy (XPS results of (c) SR-240 wood; (d) coated SR-240 wood with 60° CAs and (e) coated SR-240 wood with 152° CAs (red line: C–C/C–H; black line: C–O; blue line: C(O)O; green line: envelope); (f) XPS survey for SR-240 wood and coated SR-240 wood with 152° CAs.

### 3.4. The Robustness and Self-Replenishment of Superhydrophobic Surfaces

In practical applications, these superhydrophobic surfaces will be inevitably damaged by accidental scratches. Therefore, the surfaces mechanical resistance was firstly investigated. As shown in Figure 6a, the as-prepared superhydrophobic surface was submitted to 500 g of loading (a pressure of 3.5 KPa), while facing the 240 grit sandpaper and was moved at a distance of 10 cm per cycle. The water CA was measured after each cycle test. After nine cycles of mechanical abrasion tests, the water CAs remained unchanged with the CA hysteresis being less than 10° (Figure 6b). This means that after nine cycles of tests, the surface continued to retain its superhydrophobicity. However, the surfaces lost superhydrophobicity with the CA hysteresis larger than 10° after ten cycles of abrasion tests resulted from the damages of polymer films. These results demonstrated the acceptable resistance of the superhydrophobic surface to abrasion.

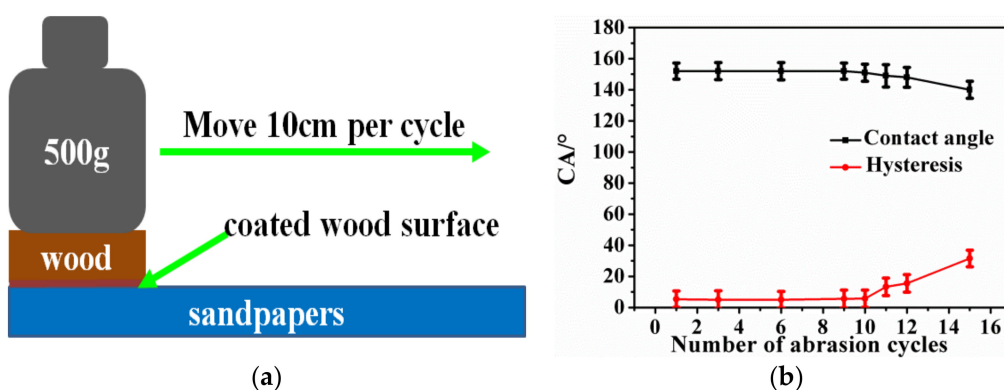


**Figure 6.** (a) Illustration of the abrasion test for the surface under 500 g of loading on sandpaper (240 grit); (b) Water CAs as a function of the number of abrasion cycles.

The superhydrophobic wood will be inevitably damaged by prolonged contact with chemicals during practical applications, such as experimental furniture. The self-replenishment of the superhydrophobic surface was examined through the soaking test in alkali and acid solutions. The superhydrophobic surface lost superhydrophobicity after it was soaked in an alkali (pH = 12) or acid (pH = 1) solution for 2 h, with the water CAs decreasing from 152° to 0°. The original superhydrophobicity of the damaged surface was recovered after it was exposed in an ambient

environment for 6 h with water CAs as  $152^\circ$  and sliding angles less than  $10^\circ$ , meaning that the surface of the damaged superhydrophobic polymer film on SR-240 wood was recovered again. Based on the intrinsic porous structures of wood surfaces, the superhydrophobic polymer film can preserve a large number of polymers as healing agents in wood pores, such as cell cavities, cell pits, and grooves. Once the primary top polymer layer is decomposed or scratched, the preserved healing agents in the cell cavities, cell pits, and grooves can migrate to the surface to heal the superhydrophobicity that is driven by the minimum interfacial energy [31]. In this way, the damaged surface would recover its superhydrophobicity at ambient temperatures when the time is long enough for the hydrophobic segments from healing agents in the pores to migrate onto the surface. As shown in Figure 7a,b, the acid and alkali etching–healing process can be repeated nine times without decreasing the superhydrophobicity of the self-healed polymer film, because the multiple porous microstructures are too robust to be destroyed, as shown in Figure 7c,d, and these are essential for the recovery of superhydrophobicity. It was found that the self-replenishment was temperature-dependent, with a more accelerated self-healing process under a higher temperature, and vice versa. When the temperature increased to 50 and  $100^\circ\text{C}$ , the time for superhydrophobicity recovery was 20 and 5 min, respectively. The higher the temperature, the faster the self-replenishment was. Therefore, the temperature participated in the self-healing process of the superhydrophobic films. The self-replenishment occurring at room temperature is important for the routine use of wood materials such as furniture and decoration materials, which are inconvenient to be heated or catalyzed by chemical agents or UV radiation. It was also found that after depleting healing agents, the self-healing ability could be restored just by spraying or casing the polymer suspensions onto wood surfaces to replenish the healing agent.

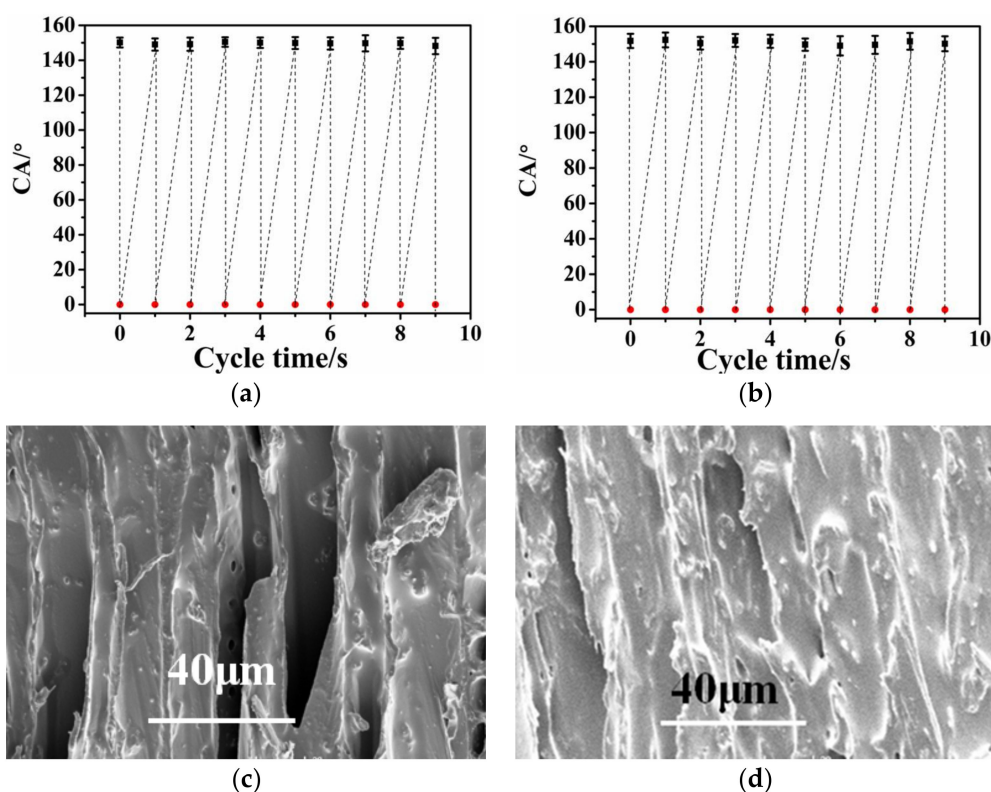


**Figure 7.** Self-replenishment of the superhydrophobic surface by (a) acid etching–healing and (b) alkali etching–healing tests. The SEM images of the etched wood surface after (c) acid etching and (d) alkali etching.

### 3.5. The Improved Water and Mildew Resistance of Wood with Superhydrophobic Surfaces

The raw wood is apt to absorb water when it is contacted with water, which will result in dimension swelling and mildew stain. The improvement in water repelling for wood could increase its water resistance and mildew inhibition greatly. After being soaked in water for 24 h, the control raw wood absorbs water quickly with the ratio of thickness expansion (C-TE), breadth expansion (C-BE), and weight growth (C-WG) as 5.4%, 2.4%, and 56%, respectively, where C stands for control raw wood (Figure 8a). The wood with superhydrophobic surfaces absorbs water much more slowly than the control raw wood with S-TE, S-BE, and S-WG as 2.9%, 2.1%, and 28.9% where S stands for superhydrophobic wood (Figure 8a). The wood with superhydrophobic surfaces absorbed water more slowly than the raw wood. The above results proved that the superhydrophobic surfaces greatly improved the water resistance of wood, which helped to inhibit the mold stains for wood, especially when it was under humid conditions for daily use. The raw wood begins to be stained by mildew at the 7th day and the whole surface is stained by mildew at the 14th days, as shown in Figure 8b. The wood with superhydrophobic surfaces is not stained by mildew at the 7th day, begins to be stained by mildew at the 14th day and approximately 75% of the surface is stained by mildew at 28th day, as shown in Figure 8b under conditions where the humidity is 90% and temperature is 30 °C. It was just the superhydrophobic surfaces that made the moisture content of the wood increase more slowly than the raw wood for the mildew to grow, which improved its mildew resistance. The superhydrophobic treatment is an environmental friendly approach to improve the mildew inhibition of wood when compared with the general method, which uses bactericidal chemical agents [51,52].

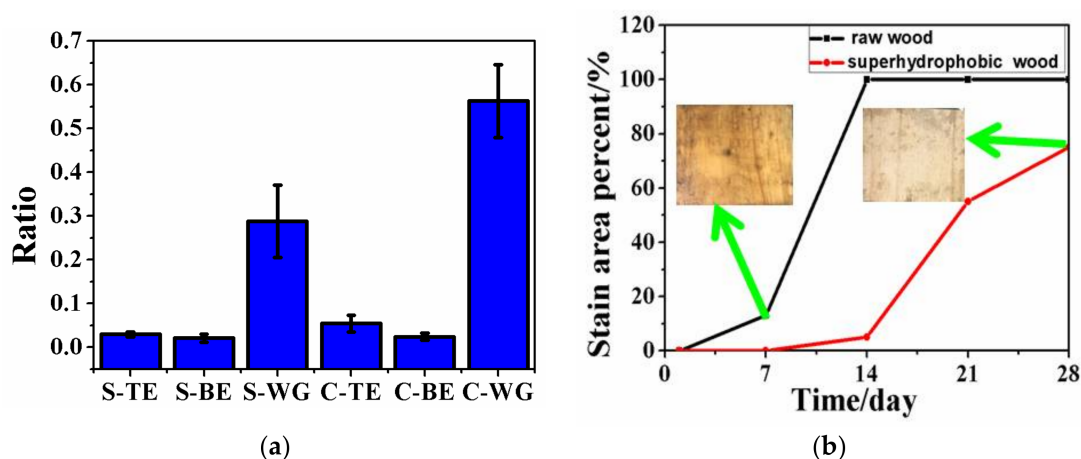


**Figure 8.** (a) The ratio of thickness expansion (TE), breadth expansion (BE), and weight growth (WG) for wood where S and C stand for superhydrophobic wood and control raw wood; (b) Mildew infection area percent for raw wood and superhydrophobic wood under humid conditions.

## 4. Conclusions

In conclusion, superhydrophobic surfaces with good resistance to abrasion have been fabricated by simply casting and drying water-soluble polymer suspensions at room temperature through polymer thermal reconstruction. On the base of the robust hierarchical microstructures that were obtained merely by sanding wood, the commonly used inorganic particles for establishing geometric microstructures were neither needed and the coating that was produced from unitary polymer was transparent. The superhydrophobic surface could self-heal superhydrophobicity at ambient temperatures and the self-healing could be accelerated at a higher temperature. After depleting the healing agents, the polymer suspension could be sprayed or cast onto wood surfaces to replenish healing agents and restore the self-healing ability. The superhydrophobic treatments greatly improve

both water resistance and mildew inhibition for wood, which extend the life expectancy and open up practical applications for wood based materials.

**Acknowledgments:** This work was supported by the National Natural Science Foundation of China (No. 51403190), National Key Project (No. 2017YFD0601105), Natural Science Foundation of Zhejiang Province of China (LY15E020011), Program for Key Science and Technology Team of Zhejiang Province (No. 2013TD17), Young Talent Cultivation Project of Zhejiang Association for Science and Technology (No. 2016YCGC019), Youth Top-notch Talent Development and Training Program Foundation of Zhejiang A&F University, Zhejiang A&F University Scientific Research Training Program for Undergraduates (No. 101-2013200038) and Jiangsu North Special Project from Jiangsu Suqian (No. BN2016176).

**Author Contributions:** Zhehong Shen and Hao Chen conceived and designed the experiments; Yalun Shen and Yitian Wu performed the experiments and analyzed the data. All authors contributed to the interpretation of the results and to the writing of the articles.

**Conflicts of Interest:** The authors declare no conflict of interest.

## References

1. Wu, M.; Ma, B.; Pan, T.; Chen, S.; Sun, J. Silver-nanoparticle-colored cotton fabrics with tunable colors and durable antibacterial and self-healing superhydrophobic properties. *Adv. Funct. Mater.* **2016**, *26*, 569–576. [[CrossRef](#)]
2. Ellinas, K.; Kefallinou, D.; Stamatakis, K.; Gogolides, E.; Tserepi, A. Is there a threshold in the antibacterial action of superhydrophobic surfaces? *ACS Appl. Mater. Interfaces* **2017**, *9*, 39781–39789. [[CrossRef](#)] [[PubMed](#)]
3. Yuan, Y.; Hays, M.P.; Hardwidge, P.R.; Kim, J. Surface characteristics influencing bacterial adhesion to polymeric substrates. *RSC Adv.* **2017**, *7*, 14254–14261. [[CrossRef](#)]
4. Zhang, X.; Wang, L.; Levanen, E. Superhydrophobic surfaces for the reduction of bacterial adhesion. *RSC Adv.* **2013**, *3*, 12003–12020. [[CrossRef](#)]
5. Wang, Y.; Shi, Y.; Pan, L.; Yang, M.; Peng, L.; Zong, S.; Shi, Y.; Yu, G. Multifunctional superhydrophobic surfaces templated from innately microstructured hydrogel matrix. *Nano Lett.* **2014**, *14*, 4803–4809. [[CrossRef](#)] [[PubMed](#)]
6. Hou, X.; Hu, Y.; Grinthal, A.; Khan, M.; Aizenberg, J. Liquid-based gating mechanism with tunable multiphase selectivity and antifouling behaviour. *Nature* **2015**, *519*, 70–73. [[CrossRef](#)] [[PubMed](#)]
7. Liu, Y.; Wang, X.; Fei, B.; Hu, H.; Lai, C.; Xin, J. Bioinspired, stimuli-responsive, multifunctional superhydrophobic surface with directional wetting, adhesion, and transport of water. *Adv. Funct. Mater.* **2015**, *25*, 5047–5056. [[CrossRef](#)]
8. Zhang, X.; Li, Z.; Liu, K.; Jiang, L. Bioinspired multifunctional foam with self-cleaning and oil/water separation. *Adv. Funct. Mater.* **2013**, *23*, 2881–2886. [[CrossRef](#)]
9. Ruan, C.; Ai, K.; Li, X.; Lu, L. A Superhydrophobic sponge with excellent absorbency and flame retardancy. *Angew. Chem.* **2014**, *126*, 5556–5560. [[CrossRef](#)] [[PubMed](#)]
10. Lu, Y.; Sathasivam, S.; Song, J.; Crick, C.R.; Carmalt, C.J.; Parkin, I.P. Robust self-cleaning surfaces that function when exposed to either air or oil. *Science* **2015**, *347*, 1132–1135. [[CrossRef](#)] [[PubMed](#)]
11. Yildirim, A.; Khudiyev, T.; Daglar, B.; Budunoglu, H.; Okyay, A.K.; Bayindir, M. Superhydrophobic and omnidirectional antireflective surfaces from nanostructured ormosil colloids. *ACS Appl. Mater. Interfaces* **2013**, *5*, 853–860. [[CrossRef](#)] [[PubMed](#)]
12. Youngblood, J.P.; McCarthy, T.J. Ultrahydrophobic polymer surfaces prepared by simultaneous ablation of polypropylene and sputtering of poly(tetrafluoroethylene) using radio frequency plasma. *Macromolecules* **1999**, *32*, 6800–6806. [[CrossRef](#)]
13. Ellinas, K.; Pujari, S.P.; Dragatogiannis, D.A.; Charitidis, C.A.; Tserepi, A.; Zuilhof, H.; Gogolides, E. Plasma micro-nanotextured, scratch, water and hexadecane resistant, superhydrophobic, and superamphiphobic polymeric surfaces with perfluorinated monolayers. *ACS Appl. Mater. Interfaces* **2014**, *6*, 6510–6524. [[CrossRef](#)] [[PubMed](#)]
14. Shon, Y.-S.; Lee, S.; Colorado, R.; Perry, S.S.; Lee, T.R. Spiroalkanedithiol-based sams reveal unique insight into the wettabilities and frictional properties of organic thin films. *J. Am. Chem. Soc.* **2000**, *122*, 7556–7563. [[CrossRef](#)]

15. Miyauchi, M.; Kieda, N.; Hishita, S.; Mitsuhashi, T.; Nakajima, A.; Watanabe, T.; Hashimoto, K. Reversible wettability control of TiO<sub>2</sub> surface by light irradiation. *Surf. Sci.* **2002**, *511*, 401–407. [[CrossRef](#)]
16. Mutel, B.; Taleb, A.B.; Dessaux, O.; Goudmand, P.; Gengembre, L.; Grimblot, J. Characterization of mixed zinc-oxidized zinc thin films deposited by a cold remote nitrogen plasma. *Thin Solid Films* **1995**, *266*, 119–128. [[CrossRef](#)]
17. Bayer, I.S.; Davis, A.J.; Loth, E.; Steele, A. Water jet resistant superhydrophobic carbonaceous films by flame synthesis and tribocharging. *Mater. Today Commun.* **2015**, *3*, 57–68. [[CrossRef](#)]
18. Bayer, I.S.; Brandi, F.; Cingolani, R.; Athanassiou, A. Modification of wetting properties of laser-textured surfaces by depositing triboelectrically charged teflon particles. *Colloid Polym. Sci.* **2013**, *291*, 367–373. [[CrossRef](#)]
19. Gu, Z.-Z.; Uetsuka, H.; Takahashi, K.; Nakajima, R.; Onishi, H.; Fujishima, A.; Sato, O. Structural color and the lotus effect. *Angew. Chem. Int. Ed.* **2003**, *42*, 894–897. [[CrossRef](#)] [[PubMed](#)]
20. Wang, J.; Wen, Y.; Feng, X.; Song, Y.; Jiang, L. Control over the wettability of colloidal crystal films by assembly temperature. *Macromol. Rapid Commun.* **2006**, *27*, 188–192. [[CrossRef](#)]
21. Wang, J.; Wen, Y.; Hu, J.; Song, Y.; Jiang, L. Fine control of the wettability transition temperature of colloidal-crystal films: From superhydrophilic to superhydrophobic. *Adv. Funct. Mater.* **2007**, *17*, 219–225. [[CrossRef](#)]
22. Latthe, S.; Terashima, C.; Nakata, K.; Sakai, M.; Fujishima, A. Development of sol-gel processed semi-transparent and self-cleaning superhydrophobic coatings. *J. Mater. Chem. A* **2014**, *2*, 5548–5553. [[CrossRef](#)]
23. Geng, Z.; He, J.; Xu, L.; Yao, L. Rational design and elaborate construction of surface nano-structures toward highly antireflective superamphiphobic coatings. *J. Mater. Chem. A* **2013**, *1*, 8721–8724. [[CrossRef](#)]
24. Chen, L.; Sun, X.; Hang, J.; Jin, L.; Shang, D.; Shi, L. Large-scale fabrication of robust superhydrophobic coatings with high rigidity and good flexibility. *Adv. Mater. Interfaces* **2016**, *3*, 500718. [[CrossRef](#)]
25. Ellinas, K.; Tserapi, A.; Gogolides, E. Durable superhydrophobic and superamphiphobic polymeric surfaces and their applications: A review. *Adv. Colloid Interface Sci.* **2017**, *250*, 132–157. [[CrossRef](#)] [[PubMed](#)]
26. Verho, T.; Bower, C.; Andrew, P.; Franssila, S.; Ikkala, O.; Ras, R.H. Mechanically durable superhydrophobic surfaces. *Adv. Mater.* **2011**, *23*, 673–678. [[CrossRef](#)] [[PubMed](#)]
27. Bayer, I.S.; Krishnan, K.G.; Robison, R.; Loth, E.; Berry, D.H.; Farrell, T.E.; Crouch, J.D. Thermal alternating polymer nanocomposite (TAPNC) coating designed to prevent aerodynamic insect fouling. *Sci. Rep.* **2016**, *6*, 38459. [[CrossRef](#)] [[PubMed](#)]
28. Li, Y.; Li, L.; Sun, J. Bioinspired self-healing superhydrophobic coatings. *Angew. Chem. Int. Ed.* **2010**, *49*, 6129–6133. [[CrossRef](#)] [[PubMed](#)]
29. Wang, H.; Xue, Y.; Ding, J.; Feng, L.; Wang, X.; Lin, T. Durable, self-healing superhydrophobic and superoleophobic surfaces from fluorinated-decyl polyhedral oligomeric silsesquioxane and hydrolyzed fluorinated alkyl silane. *Angew. Chem. Int. Ed.* **2011**, *50*, 11433–11436. [[CrossRef](#)] [[PubMed](#)]
30. Esteves, A.C.C.; Luo, Y.; Put, M.W.P.V.D.; Carcouët, C.C.M.; With, G.D. Self-replenishing dual structured superhydrophobic coatings prepared by drop-casting of an all-in-one dispersion. *Adv. Funct. Mater.* **2014**, *24*, 986–992. [[CrossRef](#)]
31. Li, Y.; Chen, S.; Wu, M.; Sun, J. All spraying processes for the fabrication of robust, self-healing, superhydrophobic coatings. *Adv. Mater.* **2014**, *26*, 3344–3348. [[CrossRef](#)] [[PubMed](#)]
32. Liu, C.; Ma, C.; Xie, Q.; Zhang, G. Self-repairing silicone coatings for marine anti-biofouling. *J. Mater. Chem. A* **2017**, *5*, 15855–15861. [[CrossRef](#)]
33. Deng, X.; Mammen, L.; Butt, H.J.; Vollmer, D. Candle soot as a template for a transparent robust superamphiphobic coating. *Science* **2012**, *335*, 67–70. [[CrossRef](#)] [[PubMed](#)]
34. Chen, K.; Zhou, S.; Yang, S.; Wu, L. Fabrication of all-water-based self-repairing superhydrophobic coatings based on UV-responsive microcapsules. *Adv. Funct. Mater.* **2015**, *25*, 1035–1041. [[CrossRef](#)]
35. Xue, C.H.; Bai, X.; Jia, S.T. Robust, self-healing superhydrophobic fabrics prepared by one-step coating of pdms and octadecylamine. *Sci. Rep.* **2016**, *6*, 27262. [[CrossRef](#)] [[PubMed](#)]
36. Yang, Y.; Urban, M.W. Self-healing polymeric materials. *Chem. Soc. Rev.* **2013**, *42*, 7446–7467. [[CrossRef](#)] [[PubMed](#)]
37. Zhu, D.Y.; Rong, M.Z.; Zhang, M.Q. Self-healing polymeric materials based on microencapsulated healing agents: From design to preparation. *Prog. Chem. Sci.* **2015**, *49–50*, 175–220. [[CrossRef](#)]

38. Chen, C.M.; Yang, S. Directed water shedding on high-aspect-ratio shape memory polymer micropillar arrays. *Adv. Mater.* **2014**, *26*, 1283–1288. [[CrossRef](#)] [[PubMed](#)]
39. Wang, W.; Salazar, J.; Vahabi, H.; Joshiimre, A.; Voit, W.E.; Kota, A.K. Metamorphic superomniphobic surfaces. *Adv. Mater.* **2017**, *29*, 1700295. [[CrossRef](#)] [[PubMed](#)]
40. Manna, U.; Lynn, D.M. Restoration of superhydrophobicity in crushed polymer films by treatment with water: Self-healing and recovery of damaged topographic features aided by an unlikely source. *Adv. Mater.* **2013**, *25*, 5104–5108. [[CrossRef](#)] [[PubMed](#)]
41. Shen, Z.; Yang, Y.; Lu, F.; Bao, B.; You, B. Self-assembly of binary particles and application as structural colors. *Polym. Chem.* **2012**, *3*, 2495–2501. [[CrossRef](#)]
42. Shen, Z.; Yang, Y.; Lu, F.; Bao, B.; You, B.; Shi, L. Self-assembly of colloidal spheres and application as solvent responding polymer film. *J. Colloid Interface Sci.* **2013**, *389*, 77–84. [[CrossRef](#)] [[PubMed](#)]
43. Bao, B.; Liu, D.; Yang, Y.; Shen, Z.; You, B. Self-assembly of ternary particles for tough colloidal crystals with vivid structure colors. *J. Nanomater.* **2013**, *2013*, 8–21. [[CrossRef](#)]
44. Cai, P.; Bai, N.; Xu, L.; Tan, C.; Li, Q. Fabrication of superhydrophobic wood surface with enhanced environmental adaptability through a solution-immersion process. *Surf. Coat. Technol.* **2015**, *277*, 262–269. [[CrossRef](#)]
45. Chang, H.; Tu, K.; Wang, X.; Liu, J. Fabrication of mechanically durable superhydrophobic wood surfaces using polydimethylsiloxane and silica nanoparticles. *RSC Adv.* **2015**, *5*, 30647–30653. [[CrossRef](#)]
46. Wang, S.; Shi, J.; Liu, C.; Cheng, X.; Wang, C. Fabrication of a superhydrophobic surface on a wood substrate. *Appl. Surf. Sci.* **2011**, *257*, 9362–9365. [[CrossRef](#)]
47. Tu, K.; Wang, X.; Kong, L.; Guan, H. Facile preparation of mechanically durable, self-healing and multifunctional superhydrophobic surfaces on solid wood. *Mater. Des.* **2018**, *140*, 30–36. [[CrossRef](#)]
48. Surface Roughness Standard (JIS B0601:1994). Available online: [https://us.misumi-ec.com/pdf/tech/mech/US2010\\_fa\\_p3541\\_3542.pdf](https://us.misumi-ec.com/pdf/tech/mech/US2010_fa_p3541_3542.pdf) (accessed on 11 March 2018).
49. Plötze, M.; Niemz, P. Porosity and pore size distribution of different wood types as determined by mercury intrusion porosimetry. *Eur. J. Wood Wood Prod.* **2011**, *69*, 649–657. [[CrossRef](#)]
50. Sperry, P.R.; Snyder, B.S.; O'Dowd, M.L.; Lesko, P.M. Role of water in particle deformation and compaction in latex film formation. *Langmuir* **1994**, *10*, 2619–2628. [[CrossRef](#)]
51. Ruhs, C. Developing environmentally benign and effective organic wood preservatives by understanding the biocidal and non-biocidal properties of extractives in naturally durable heartwood. *Holzforschung* **2008**, *62*, 264–269. [[CrossRef](#)]
52. Schultz, T.P.; Nicholas, D.D. Development of environmentally-benign wood preservatives based on the combination of organic biocides with antioxidants and metal chelators. *Phytochemistry* **2002**, *61*, 555–560. [[CrossRef](#)]

